Received: 15 December 2019 | Revised: 13 February 2020 | Accepted: 19 February 2020

DOI: 10.1096/fj.201902982R

RESEARCH ARTICLE

THE FASEB JOURNAL

PKA-independent vasopressin signaling in renal collecting duct

Arnab Datta[1,2] | **Chin-Rang Yang**[1] | **Kavee Limbutara**[1] | **Chung-Lin Chou**[1] | **Markus M. Rinschen**[3] | **Viswanathan Raghuram**[1] | **Mark A. Knepper**[1]

[1]Epithelial Systems Biology Laboratory, Systems Biology Center, National Heart, Lung, and Blood Institute, National Institutes of Health, Bethesda, MD, USA

[2]Yenepoya Research Center, Yenepoya (Deemed to be University), Mangalore, India

[3]Department of Chemistry, Center for Metabolomics and Mass Spectrometry, The Scripps Research Institute, La Jolla, CA, USA

Correspondence
Mark A. Knepper, Epithelial Systems Biology Laboratory, Systems Biology Center, National Heart, Lung, and Blood Institute, National Institutes of Health, Bethesda, MD 20892, USA.
Email: knep@helix.nih.gov

Funding information
HHS | NIH | National Heart, Lung, and Blood Institute (NHLBI), Grant/Award Number: ZIA-HL-001285; HHS | NIH | National Heart, Lung, and Blood Institute (NHLBI), Grant/Award Number: ZIA-HL-006129

Abstract

Vasopressin regulates renal water excretion by binding to a $G_{\alpha}s$-coupled receptor (V2R) in collecting duct cells, resulting in increased water permeability through regulation of the aquaporin-2 (AQP2) water channel. This action is widely accepted to be associated with cAMP-mediated activation of protein kinase A (PKA). Here, we use phosphoproteomics in collecting duct cells in which PKA has been deleted (CRISPR-Cas9) to identify PKA-independent responses to vasopressin. The results show that V2R-mediated vasopressin signaling is predominantly, but not entirely, PKA-dependent. Upregulated sites in PKA-null cells include Ser256 of AQP2, which is critical to regulation of AQP2 trafficking. In addition, phosphorylation changes in the protein kinases Stk39 (SPAK) and Prkci (an atypical PKC) are consistent with PKA-independent regulation of these protein kinases. Target motif analysis of the phosphopeptides increased in PKA-null cells indicates that vasopressin activates one or more members of the AMPK/SNF1-subfamily of basophilic protein kinases. In vitro phosphorylation assays using recombinant, purified SNF1-subfamily kinases confirmed postulated target specificities. Of interest, measured IBMX-dependent cAMP levels were an order of magnitude higher in PKA-null than in PKA-intact cells, indicative of a PKA-dependent feedback mechanism. Overall, the findings support the conclusion that V2-receptor mediated signaling in collecting duct cells is in part PKA-independent.

KEYWORDS

AMPK, AQP2, cAMP, mpkCCD, phosphoproteomics, PRM-MS

1 | INTRODUCTION

Body water balance is regulated chiefly by the peptide hormone vasopressin, which acts in the kidney to control the rate of water excretion.[1] Vasopressin regulates water excretion chiefly by controlling the osmotic water permeability of collecting duct cells through changes in the abundance and cellular distribution of the water channel aquaporin-2 (AQP2).[2] The permeability changes, therefore, determine whether luminal water is returned to the general circulation (high vasopressin) or excreted in the urine (low vasopressin). The regulation of osmotic water transport in the renal

Abbreviations: AQP2, aquaporin-2; dDAVP, D-amino D-arginine vasopressin; EThcD, electron-transfer/higher-energy collision dissociation; FA, formic acid; GPCR, G-protein coupled receptor; HCD, higher-energy collisional dissociation; IBMX, 3-isobutyl-1-methylxanthine; nLC-MS/MS, nano liquid chromatography-tandem mass spectrometry; PKA, protein kinase A; PRM, parallel reaction monitoring; SILAC, stable-isotopic labeling with amino acids in cell culture; V2R, vasopressin V2 receptor.

collecting duct is accomplished largely through two mechanisms: (a) control of membrane-trafficking, which carries AQP2 water channels to and from the apical plasma membrane [3,4]; and (b) control of transcription of the *Aqp2* gene,[5-7] which codes for AQP2.[8]

Signaling pathways responsible for vasopressin action in renal collecting duct cells are incompletely understood. What is known is that vasopressin binds to a G-protein coupled receptor (GPCR), namely the vasopressin V2 receptor (V2R), which activates adenylyl cyclase through the heterotrimeric G-protein α subunit $G_{\alpha}s$, thereby increasing intracellular cyclic-AMP (cAMP). Although cAMP can act in the cell via other effectors, it is generally believed that protein kinase A (PKA) is responsible for vasopressin's effects on AQP2 trafficking and transcription. This view was supported by recent studies in which both genes coding for PKA catalytic subunits were deleted in cultured collecting duct cells (mpkCCD).[9] Although these PKA-null cells grew well and maintained their normal epithelial polarity, both apical trafficking of AQP2 and transcription of the *Aqp2* gene were virtually completely ablated, implying that PKA is important for AQP2 regulation by vasopressin. However, whether vasopressin exerts some of its actions through PKA-independent signaling pathways is thus far unclear.

In our previous paper,[9] we compared vasopressin-treated PKA-null cells with vasopressin-treated PKA-intact cells, but did not investigate phosphoproteomic responses to vasopressin in these two cell lines. To identify vasopressin-dependent signaling pathways in PKA-intact and PKA-null mpkCCD cells, we have now carried out large scale phosphoproteomic analysis using quantitative protein mass spectrometry. The data allowed us to create two publicly accessible online databases (for vasopressin responses in PKA-intact and PKA-null cells, respectively) to serve as resources for future studies of V2R signaling and signaling mediated by other $G_{\alpha}s$-coupled receptors. The data in PKA-null cells allowed identification of several protein kinases, viz., SPAK (Stk39), PKC-iota (Prkci), and one or more members of the SNF1-subfamily of protein kinases, as regulated targets of vasopressin in the absence of PKA. In vitro nLC-MS/MS-based phosphorylation assays using recombinant, purified protein SNF1-subfamily kinases confirmed postulated target specificities.

2 | MATERIALS AND METHODS

2.1 | Reagents

Unless mentioned otherwise, all chemicals and reagents except the one used for proteomics sample preparation were purchased from Sigma (St. Louis, MO). The reagents used for proteomics sample preparation and nLC-MS/MS analysis were purchased from Thermo Fisher Scientific (Waltham, MA) unless stated otherwise.

2.2 | Cell lines

Three clones each of PKA-null and PKA-intact mouse kidney collecting duct cell lines, derived from *mpk*CCD clone 11-38 ($mpkCCD_{C11\text{-}38}$) using CRISPR-Cas9 to introduce mutations were used for this study.[9] All experiments were performed with passages from 10 to 20 relative to the production of the original CRISPR clones.

2.3 | Cell culture

Cells were maintained in complete medium containing DMEM/Ham's F-12 medium (DMEM/F-12), 2% (v/v) FBS plus supplements (5 μg/mL insulin; 50 nM dexamethasone; 1 nM triiodothyronine; 10 ng/mL epidermal growth factor; 60 nM sodium selenite; 5 μg/mL transferrin) at 37°C and 5% (v/v) CO_2. For all experiments, cells were seeded onto permeable membrane supports (Transwell, 0.4 μm Polyester membrane; cat. no. 3450)(Corning Costar, Corning, NY) with complete media for 4-7 days to allow the formation of a confluent epithelial monolayer with cell polarization. Then, the media were changed to serum-free simple media (DMEM/F12 containing 50 nM dexamethasone, 60 nM sodium selenite, and 5 μg/mL transferrin) for 3 days to induce cellular differentiation and to ensure complete polarization. Except where indicated, the basolateral medium was identical with the apical media except for the addition of 0.1 nM of the vasopressin analog, D-amino D-arginine vasopressin (dDAVP). Transepithelial resistances were measured by voltmeter (EVOM2, WPI, Sarasota, FL). The apical and basolateral media were changed daily.

2.4 | Stable-isotopic labeling with amino acids in cell culture (SILAC) and short-term dDAVP stimulation

The cells were labeled by growing in complete SILAC medium (Thermo Fisher) containing either heavy ($^{13}C_6{}^{15}N_4$ arginine and $^{13}C_6$ lysine) and light ($^{12}C_6{}^{14}N_4$ arginine and $^{12}C_6$ lysine) amino acids. The cells were cultured for 17 days (five passages) to reach >99.9% labeling.[10] Heavy- or light-labeled cells were then grown on separate 6-well Transwell plates (containing labeled amino acids) for 7 days in complete SILAC medium and for 3 days in simple SILAC medium in the presence of dDAVP (0.1 nM) in basolateral media. On the 10th day, following a 2 hour dDAVP wash-out period, light-labeled and heavy-labeled plates were treated with 0.1 nM dDAVP or vehicle,

respectively, for 30 minutes. The cells were washed with PBS and stored immediately at −80°C until further processing.

2.5 | Sample preparation for total proteomics and phosphoproteomics

The cells were thawed on ice and treated with urea buffer (8 M urea, 50 mM Tris·HCl, 75 mM NaCl, 1 × Halt protease and phosphatase inhibitors), scraped and sonicated (duration: 2 min, pulse/pause: 2 s/2 s, output level = 1) to solubilize proteins. Following measurement of protein concentration (BCA reagent), equal amounts of heavy- and light-labeled protein extracts were mixed (total, 2.5 ± 0.4 mg). The mixed samples were reduced with 20 mM DTT for 1 hour at 37°C, and then alkylated with 40 mM iodoacetamide for 1 hour at 25°C in the dark. The samples were diluted with 20 mM triethylammonium bicarbonate buffer (pH 8.5) to 1 M urea, and then digested with trypsin/LysC (Promega, Madison, WI) (1:20 wt/wt) overnight at 37°C. The peptides were desalted using hydrophilic–lipophilic–balanced extraction cartridges (Oasis, 1 cc, 30 mg). The peptide sample was divided into three parts: total peptide analysis (4%), heretofore referred to as "Total" and phosphopeptide enrichments (48% × 2) using Fe-NTA (High-Select Fe-NTA Phosphopeptide Enrichment Kit, Cat. No.: 88300) and TiO_2 columns (High-Select TiO_2 Phosphopeptide Enrichment Kit, Cat No.: A32993). The enrichment protocols were as described in the manufacturer's instructions with minor modifications. The enriched peptides from Fe-NTA columns were desalted using graphite columns (Pierce Graphite Spin Columns, Cat. No.: 88302). All three samples (Total, TiO_2, Fe-NTA) were fractionated in a 96-well plate with off-line high-pH reverse-phase chromatography (Agilent 1200 HPLC system, Santa Clara, CA) using a XBridge BEH C18 column (Waters, Milford, MA; 130 Å, 5 μm, 2.1 × 30 mm). A flow rate of 0.5 mL/min was used to generate the gradient with buffer A (10 mM TEAB) and buffer B (10 mM TEAB, 90% acetonitrile [ACN]). For each SILAC experiment, eluted samples were concatenated using a discontinuous scheme to 24 (Total), 12 (TiO_2) and 12 (Fe-NTA) fractions, vacuum-dried, and stored at −80°C. The dried peptides were reconstituted with 0.1% (v/v) formic acid (FA) in LC-MS–grade water (JT Baker, Fisher Scientific) before mass spectrometry analysis.

2.6 | Nano liquid chromatography-tandem mass spectrometry (nLC-MS/MS)

Reversed-phase capillary HPLC separations were performed using a Dionex UltiMate 3000 RSLC nanosystem coupled in-line with an Orbitrap Fusion Lumos Tribrid mass spectrometer. Approximately 1.2 μg of peptides (calculated from digested cell lysate) were loaded onto the trapping column (PepMap100, C18, 75 μm × 2 cm), for 8 minutes at a flow rate of 5 μL/min with buffer A (0.1% [v/v] FA). The trapped peptides were fractionated on an analytical column (PepMap RSLC C18, 2 μm, 100 Å, 75 μm i.d. × 50 cm) using a gradient of buffer B (ACN, 0.1% (v/v) FA) as follows: 4%-22% for 83 minutes; 22%-32% for 17 minutes; 32%-90% for 3 minutes; followed by 90% buffer B for 7 minutes. The method duration was 120 minutes. Phosphopeptide-enriched samples were injected one each for higher-energy collisional dissociation (HCD) and electron-transfer/higher-energy collision dissociation (EThcD) fragmentation while "Total" samples were analyzed by HCD fragmentation only.

2.7 | HCD fragmentation

MS(/MS) data were acquired on an Orbitrap Fusion as follows: All MS1 spectra were acquired over m/z 375 − 1500 in the orbitrap with a resolution of 120 000 (FWHM) at m/z 200; automatic gain control was set to accumulate 4×10^5 ions, with a maximum injection time of 50 ms. The intensity threshold for fragmentation was set to 25 000 and included charge states +2 to +5. A dynamic exclusion of 15 seconds was applied with a mass tolerance of 7 ppm. Data-dependent tandem MS analysis was performed using a top-speed approach and the dynamic parallelization using "ADAPT" technology. The isolation window (m/z) was set at 1.6. HCD collision energy was set at 30%. MS2 spectra were acquired with Orbitrap resolution of 30 000 and a fixed first m/z of 110. Automatic gain control target was set to 5×10^4, with a maximum injection time of 60 ms. The cycle time was 3 seconds.

2.8 | EThcD fragmentation

Most of the MS(/MS) parameters for EThcD was identical as HCD fragmentation except the following: The charge states for fragmentation range from +3 to +7. ETD calibrated charge-dependent parameters and ETD supplemental activation was applied for data-dependent tandem MS. Supplemental activation collision energy for EThcD was set at 15%. Automatic gain control was set to 5×10^4, with a maximum injection time of 120 ms.

2.9 | MS raw data analysis

Raw data were analyzed using Proteome Discoverer 1.4 (version 1.4.0.288) in conjunction with two search engines; Mascot and SequestHT. The protein database used for SequestHT was the mouse Swiss-Prot (downloaded on April 16, 2017). The Mascot search engine and database were

maintained by NIH Mascot server (https://biospec.nih.gov). The search criteria for all HCD raw files were set as follows: (a) precursor mass tolerance = 10 ppm, (b) fragment mass tolerance = 0.02 Da, (c) enzyme specificity was set as trypsin with two missed cleavages allowed. Carbamidomethylation of cysteine (C + 57.021 Da) was set as a fixed modification. Variable modifications were as follows: (a) isotope labeling of lysine (K + 6.020 Da) and arginine (R + 10.008 Da), (b) oxidation of methionine (M + 15.995 Da), (c) deamination on glutamine and asparagine (N, Q + 0.984 Da), (d) phosphorylation of serine, threonine, and tyrosine (S, T, Y + 79.966 Da), and (e) acetylation of protein N-terminal. The FDR was calculated by the target-decoy algorithm.

The search parameters for raw data files generated through EThcD fragmentation were kept identical except following modifications: (a) precursor selection: "use MS(n-1) precursor" instead of "use MS1 precursor"; (b) maximum precursor mass: 8000 Da instead of 5000 Da; (c) total intensity threshold: 0 instead of 1000; (d) maximum missed cleavage sites: 3. In addition, for SequestHT search, "c" and "z" ions were used for spectral matching instead of "b" and "y" ions that were used for HCD raw files.

The probabilities of the phosphorylation site localizations were calculated based on the given MS2 data using the *PhosphoRS 3.0* module within Proteome Discoverer. The following data reduction filters were used; peptide confidence: high, peptide rank = 1. The FDR was calculated by the target decoy PSM validator. The FDR was set <.01.

2.10 | Data integration across biological replicates

For "Total" proteomics, the SequestHT and Mascot search results of three SILAC experiments corresponding to three clones each (biological replicate = 3) of PKA-intact and PKA-null cells were integrated in Proteome Discoverer after disabling the "protein grouping" option. The ratio (dDAVP/Vehicle) obtained by SequestHT was used when available. Otherwise, the ratio generated by Mascot was taken. The proteins that were quantified in all three biological replicates were used for further analysis. Paired *t* tests were used to calculate *P* values for comparison of $\log_2$[dDAVP/Vehicle] ratios versus $\log_2$[1] (null hypothesis). The median of log-ratios was reported along with corresponding *P* value.

For phosphoproteomics of PKA-intact and PKA-null cells, ".msf" files of TiO_2 and Fe-NTA samples searched with Mascot and SequestHT for all three SILAC experiments were integrated in Proteome Discoverer that resulted in two combined files, one each for HCD and EThcD fragmentation. The peptides in the combined file were grouped by "mass and sequence" available with Proteome Discoverer. The phosphopeptides having an area (MS1 scan) of at least 1.0E7 in each of the replicate cell clones along with a corresponding median ratio calculated from TiO_2 and Fe-NTA results were considered for further analysis. The phosphopeptides with a greater than 80% of phosphorylation site-assignment probability were selected. Amino acid sequences of these phosphopeptides were centralized around the phosphorylation site using PTM Centralizer (https://hpcwebapps.cit.nih.gov/ESBL/PtmCentralizer/). To account for biological variation across three replicates, (a) the phosphopeptides having three "dDAVP/Vehicle" ratios out of three SILAC experiments; (b) showing consistent direction of regulation were considered for further analysis. The data files obtained from HCD and EThcD fragmentation were combined and median phosphorylation of site-specific ratios was calculated from all monophosphopeptides representing the same phopsho-site. Dual criteria were used to identify phospho-sites with altered abundance, namely, $|\log_2(\text{dDAVP/vehicle})| > .378$ and $P_{fp} < .005$. A value of 0.378 was assigned to encompass 95% of $\log_2$(control/control) values (95% confidence interval for control-to-control comparisons).[11] P_{fp} (a measure of false positive probability) for phosphopeptide quantification was calculated as a product of the *P* value from the *t*-statistic using all three pairs of dDAVP-vehicle replicates and the area under the Gaussian distribution curve outside the range $[-Z, Z]$, where *Z* is the value divided by the SD of $\log_2$(control/control) values. *PTM-Logo* was used to generate sequence logos.[12] The inputs were 13-mer centralized sequences around the phosphorylation site.

2.11 | Cyclic AMP measurement

For short-term vasopressin stimulation, dDAVP-conditioned cells on 6-well Transwell plates in simple media in the absence of dDAVP for 2 hours (wash-out phase) on the day of experiment were treated with IBMX (3-isobutyl-1-methylxanthine, 0.5 mM on both apical and basolateral media) and concurrently with either 0.1 nM dDAVP or vehicle for 30 minutes (in the basolateral medium only). The experiments were performed in triplicate for each of three clones of PKA-intact and PKA-null cells. After incubation, the cells were rapidly washed with ice-cold PBS and frozen at −80°C. For another set of parallel experiment, IBMX was omitted.

Cyclic-AMP content was measured using the cAMP enzyme immunoassay kit (Cayman Biochemical) according to the manufacturer's instructions. Briefly, the cells were lysed using 0.1 M HCl and centrifuged to collect the supernatant. The protein content of the samples was measured by BCA assay. The samples were diluted 10 times with ELISA buffer (provided in kit) before estimating the cAMP concentration in duplicate using standards provided in the kit. The amount of cAMP was inversely proportional to the optical density measured. Results are expressed as pmol/mg protein. Data are represented as mean ± standard deviation.

2.12 | Protein kinase prediction

The Group-based Prediction System (GPS 3.0, http://gps.biocuckoo.org) was used to predict probable kinases based on the substrate sequence motifs.[13] The FASTA sequences of the proteins were uploaded using the "batch predictor" option in GPS 3.0—species-specific, where "mouse" was selected as "organism". "Tyrosine Kinase" was excluded from the analysis. The most stringent threshold (ie "High") for the cut-off for false-positive rate was chosen. This corresponds to 2% false-positive rates for kinases while making predictions on large-scale data. The site-specific scores for predicted kinases were calculated as the "score difference" between the actual score and cut-off value. For prediction of multiple probable kinases for a phospho-site, only the top hit having the maximum "score difference" was used for subsequent analysis.

2.13 | Immunoblot analysis

Laemmli buffer (2% SDS, 63 mM Tris, pH 6.8, protease and phosphatase inhibitors) was used to solubilize the cellular proteins. Protein concentration was measured using the BCA assay. The denatured samples were subjected to SDS/PAGE. The proteins were transferred to nitrocellulose membranes and probed with primary antibodies from Cell Signaling Technology (Danvers, MA) at indicated dilutions: anti-AMPKα (1:1000, isotype: Rabbit, Cat. No. 5832), anti-phospho AMPKα (Thr172) (1:1000, isotype: Rabbit IgG, Cat. No. 50081). REVERT total protein stain, blocking buffer, and infrared fluorescence-conjugated secondary antibodies were obtained from LI-COR. Fluorescence images were visualized by a LI-COR Odyssey System (ODY-0428). Band intensities were analyzed by LI-COR Image Studio software.

2.14 | In vitro phosphorylation assay

Synthetic and nonphosphorylated 13-mer peptides centralized around the increased phosphorylation sites in Crtc1 (S151, SWRRTNS*DSALHQ), Lipe (S559, SMRRSVS*EAALAQ) and Arhgef2 (S151, SLAKSVS*TTNIAG) were synthesized (FDA, White Oak, MD). AMARA (ab204852, Abcam, Cambridge, MA) and SAMS-tide (ab120182) were used as standard peptides for SIK and AMPK phosphorylation. All SNF1-subfamily enzymes (AMPK, MARK3, QIK (SIK2), NUAK2, and MELK) were purchased from Carna Biosciences (Chuo-ku, Kobe, Japan). Recombinant AMPK (AMPKα1β1γ1, AMPKα2β2γ1, AMPKα2β1γ1) was custom-made without phosphorylation at T183 (in AMPKα1) or T172 (in AMPKα2). All peptides (custom peptides, 20 nmol; standard peptides, 10 nmole) were incubated with various purified enzymes individually (ie AMPK, SIK2) in kinase reaction buffer (25 mM MOPS, 25 mM $MgCl_2$, 2 mM EDTA, 12.5 mM β-glycerol-phosphate) and supplemented with 100 μM ATP and 0.25 mM DTT for 1 hour at 30°C (all components were from Signal Chem, Richmond, BC, Canada). AMP (0-100 μM) (Signal Chem) and cAMP (0-1000 μM) were added in different concentrations as mentioned in Figure legands. The enzyme concentration was 2-4 ng/μL. The optimum concentration was determined based on the enzyme activity data provided by the manufacturer. The enzymatic reaction was terminated by centrifuging (14 000 *g*, 10 min) the reaction mixture in a 30K molecular weight cut-off filter (Amicon Ultra, Milipore) to retain the enzymes, while the phosphorylated peptides are collected as filtrate. The filtrate was diluted in 0.1% FA, 2% ACN for MS analysis in a parallel reaction monitoring (PRM) mode.

2.15 | PRM mass spectrometry

The Orbitrap Fusion Lumos Tribrid MS instrument was used in a PRM mode. The total method duration was 52 minutes. The data type was set as "profile" with "positive" polarity and source fragmentation was disabled for both MS1 and MS2 scans. All MS1 master scans were acquired over a scan range (m/z) 375-850 in the orbitrap with a resolution of 120 000 (FWHM) at m/z 200. Automatic gain control was set 1.0e6, with a maximum injection time of 100 ms.

For targeted MS2 (tMS^2) scan, the pre-defined precursor ions were selected in quadrupole mode with an isolation window of 0.7 m/z. The ions were fragmented by CID with a CID collision energy 35% and CID activation time 10 ms. The fragment ions were detected using orbitrap mass analyzer with following settings: orbitrap resolution: 50 000, mass range: normal, scan range (m/z): 200-1300, RF lens (%): 30, automatic gain control: 2.0e5. The cycle time was set as 3 seconds. The precursor m/z and charge (z) for all peptides with and without phosphorylation can be found in the Supporting Table 1.

2.16 | PRM data analysis with Skyline

Raw data were processed on an open-source software, Skyline (version 4.2.0. 19072) (https://skyline.ms/project/home/software/Skyline/begin.view).[14] Briefly, the peptide sequences were added manually to skyline. The peptide and transition settings were updated as mentioned. In transition setting, peptides with a precursor charge of 2-4, ion charge of 1-3 and ion types of b, y, and p (precursor) were used for filtering all ions. The ion match tolerance was set as 0.02 m/z for peak extraction. In full scan tab, orbitrap was selected as precursor and product mass analyzer. The acquisition method was set as targeted under MS/MS filtering. All

matching scans were included for retention time filtering. Subsequently, MS data files were imported into the software. Based on the incorporated parameters, the software extracts the chromatogram peaks and auto-calculates the charge state, retention time, background-subtracted chromatogram area, and background for all precursor and corresponding productions. The retention time window of used chromatograms was manually verified and adjusted among different samples to avoid sample-specific bias, if any. The corrected chromatogram area of precursors and diagnostic product ions was used for the final analysis. Phosphorylation was measured from the chromatogram area of the mono-phosphorylated precursor ion of specific peptides. The site of phosphorylation was determined by measuring the intensity of the site-specific fragment ion (ie diagnostic product ion) and/or corresponding neutral loss (ie diagnostic neutral loss). Phosphorylation increases the precursor mass by 79.96, while neutral loss decreases the product ion mass by 98.[15] The product ions from the y-series were used for the area measurement.

2.17 | Statistical analysis

Data were analyzed with GraphPad Prism and "data analysis" add-in of Microsoft excel software. The statistical methods used, indexed to figures in the main text, are as follows. Data for cAMP and immunoblot measurement were analyzed using a two-tailed independent samples *t*-test (*$P < .05$). Over-representation of a specific amino acid (amino acid frequency) was subjected to chi-square analysis ($\chi^2\alpha < .01$).

3 | RESULTS

3.1 | Quantitative phosphoproteomics of PKA-null and PKA-intact collecting duct cells

The mpkCCD cell line has been previously shown to exhibit vasopressin-responses (AQP2 trafficking and AQP2 transcriptional regulation) typical of native collecting duct cells.[16] CRISPR-Cas9 genome editing was previously used to create multiple lines of PKA-null cells and control PKA-intact cells allowing us to generate true biological replicate experiments using the different lines.[9] To identify phosphorylation changes in the PKA-null and PKA-intact mpkCCD cells in response to the V2-selective vasopressin analog dDAVP, we carried out quantitative phosphoproteomics using SILAC for quantification (see Section 2). In general, total protein abundances did not change in response to dDAVP (30 min) in either PKA-null or -intact cells, based on analysis of aliquots prior to phosphopeptide enrichment (Supporting Figure S1). To maximize the depth of phosphopeptide identification, enriched samples were subjected to two different fragmentation methods (HCD and EThcD). In the PKA-null cells, we quantified 13 275 unique phosphopeptides (2479 phosphoproteins) using HCD and 5789 unique phosphopeptides (1502 phosphoproteins) with EThcD fragmentation, based on filtering criteria described in Section 2 (Figure 1). For PKA-intact cells, using an identical criterion, 17 336 unique phosphopeptides (2930 phosphoproteins) were quantified using HCD and 7173 unique phosphopeptides (1722 phosphoproteins) were quantified with EThcD fragmentation (Figure 1). Overall, addition of EThcD increased the coverage

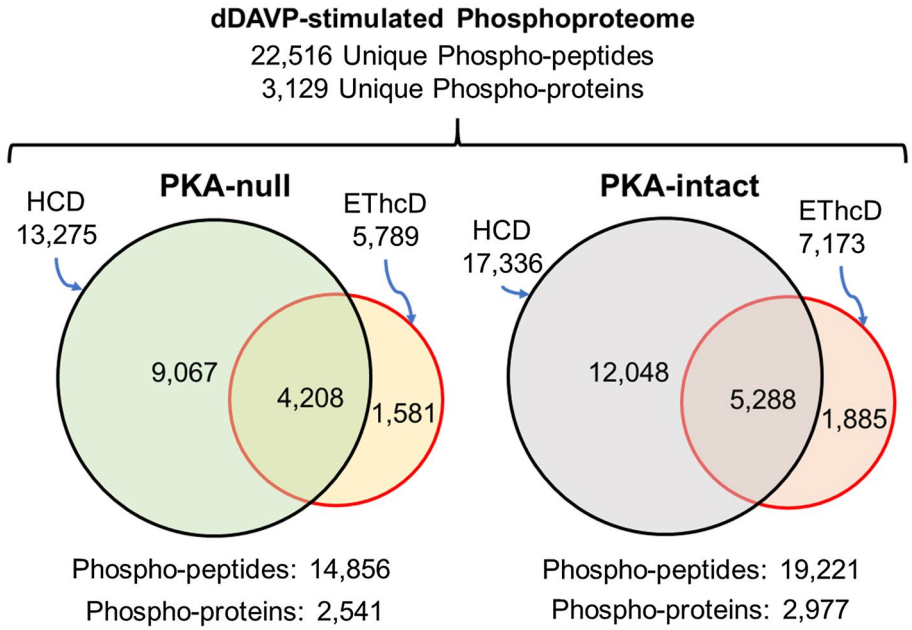

FIGURE 1 Venn diagrams comparing unique phosphopeptides and phosphoproteins identified by SILAC-based quantitative phosphoproteomics analysis in dDAVP-stimulated PKA-null and -intact cells using HCD and EThcD fragmentation. These phosphopeptides were identified (a) in all three biological replicates for receptive cell-types (b) with a minimum spectral area (MS1 scan) of at least 1.0E7. Peptide FDR was <.01

of unique phosphopeptide identification by about 10% beyond what would have been obtained with HCD alone. Single-, double-, triple-, and higher-phosphorylated peptides represented 79%, 18%, 3% and <1% of the total phosphopeptides, respectively. We observed mostly serine phosphorylation (PKA-null, 91.5%; PKA-intact, 90.7%), followed by threonine (PKA-null, 8.3%; PKA-intact, 9.0%), and tyrosine (PKA-null, 0.2%; PKA-intact, 0.3%) phosphorylation. The curated data set for quantified phosphopeptides in the PKA-null cells can be viewed at https://hpcwebapps.cit.nih.gov/ESBL/Database/PKA-null/index.html. Curated data set for quantified phosphopeptides in PKA-intact cells can be viewed at https://hpcwebapps.cit.nih.gov/ESBL/Database/PKA-Intact/index.html.

3.2 | AQP2 phosphorylation in response to vasopressin in PKA-null cells

Prior studies indicate that vasopressin stimulation increases phosphorylation of AQP2 at S256.[17] To provide confirmation that the cells are responding appropriately to vasopressin in the current experiments, we show the AQP2-S256 MS1 spectra from one SILAC experimental PKA-intact pair before (heavy) and after (light) dDAVP exposure (Figure 2A). Overall, dDAVP caused a consistent increase in phosphorylation at S256 [$\log_2$(dDAVP/Vehicle) = 1.44, $P < .05$, n = 3]. Thus, the PKA-intact cells appear to be responding to dDAVP stimulation as expected. Interestingly, AQP2 was seen to be phosphorylated at S256 in the PKA-null cells as well (Figure 2B). Furthermore, the phosphorylation increased in response to dDAVP [$\log_2$(dDAVP/Vehicle) = 0.63, $P < .05$] for all mono-S256 phosphopeptides [n = 6 pairs] (Supporting Table S1). Taken together, we conclude that (a) both PKA-intact and -null cells respond to short-term vasopressin stimulation; and (b) S256 of AQP2 can be phosphorylated and regulated in response to vasopressin even in the absence of PKA.

3.3 | Major elements of V2 vasopressin receptor signaling are PKA-dependent

Figure 3A,B summarizes abundance changes for phosphorylation sites ascertained from mono-phosphopeptides in response to the V2-selective agonist dDAVP in PKA-intact cells and PKA-null cells. The threshold for identifying a phosphopeptide as "changed" is defined as $P_{fp} < .01$ (calculated as described in Section 2). In the PKA-intact cells, dDAVP addition resulted in significant perturbations at 452 sites (in 366 distinct proteins) out of 3748 quantified (12%). Of these, 205 were increased and 247 were decreased. In the PKA-null cells, there were also changes in the phosphoproteome although there were fewer altered phosphorylation sites than in PKA-intact cells. Overall, in the PKA-null cells,

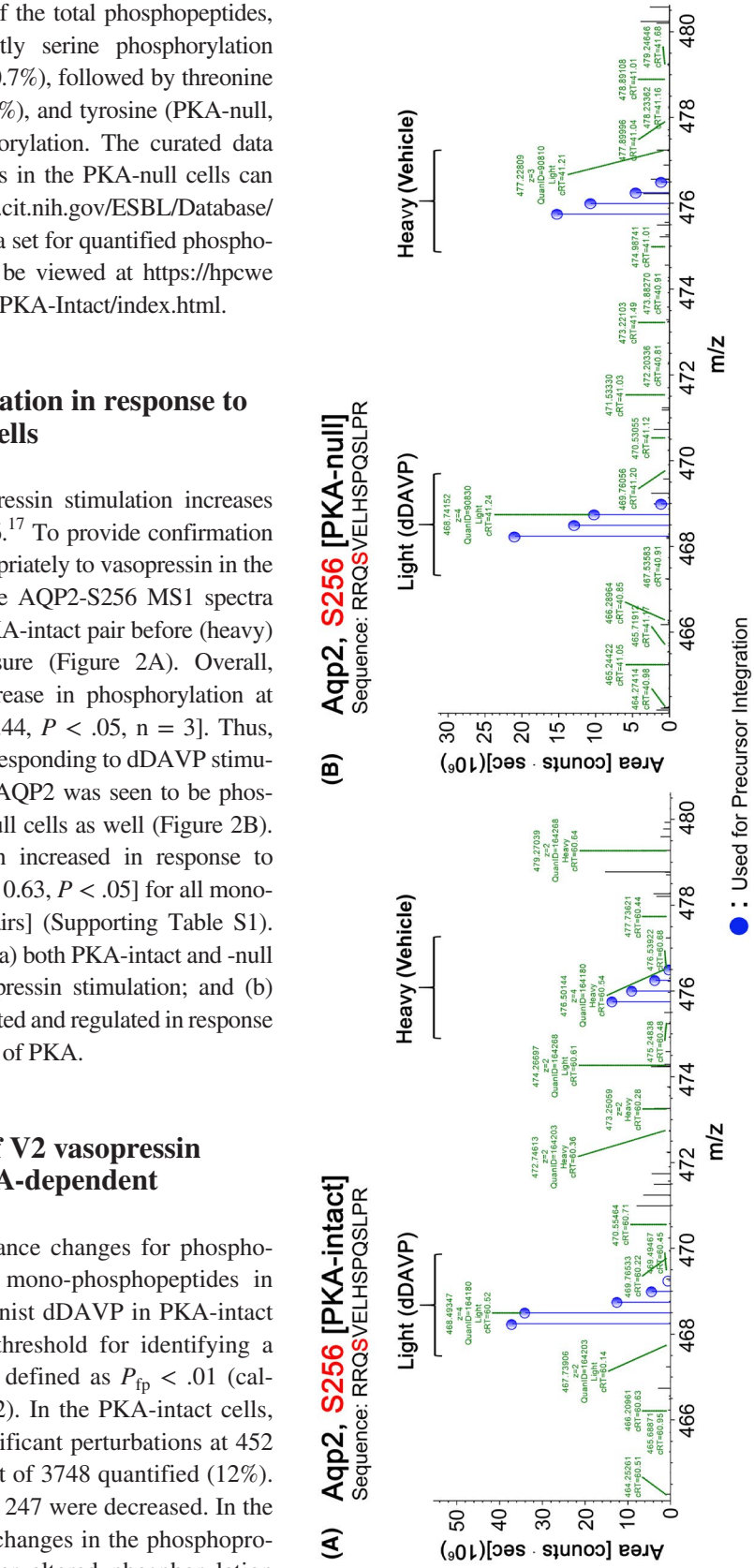

FIGURE 2 Representative MS1 spectra of Ser256 phosphopeptide of AQP2 showing an increase in dDAVP-treated (labeled with light amino acids) samples compared to vehicle treated or control (labeled with heavy amino acids) samples of (A) PKA-intact and (B) PKA-null cells. The phosphorylation site was marked in red in the peptide sequence. The vertical axis shows peptide ion intensity, and the horizontal axis shows the mass-to-charge ratio (m/z). Each peptide has several m/z peaks due to the presence of natural isotopes

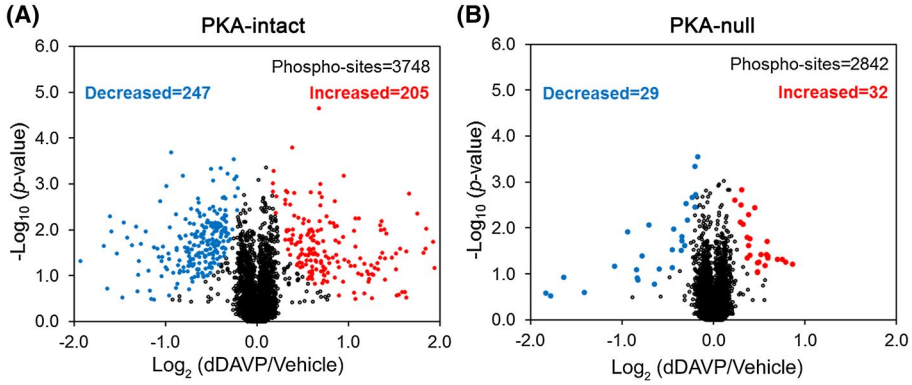

FIGURE 3 Volcano plot for single and unique phosphorylation sites quantified with a consistent trend across all three pairs (dDAVP vs vehicle) of (A) PKA-intact and (B) PKA-null clones. Phosphosites having a site-assignment probability >80% as determined by PhosphoRS 3.0 were used for this analysis. The red and blue dots indicate increased and decreased phosphorylation sites with $P_{fp} \leq .01$. The plots were presented with an x-axis value of −2.0 to +2.0 for better visualization

there were changes in 2.2% (61/2842) of quantified phosphosites (Figure 3). Of these, 32 were increased and 29 were decreased. Analysis of multiply phosphorylated peptides also showed many more regulated phosphopeptides in the PKA-intact cells than in PKA-null cells (Supporting Figure S2).

Although the preceding data establish that most of the phosphorylation changes in mpkCCD cells in response to vasopressin are PKA-dependent, PKA-independent changes were also observed. To assess the quality of these data, we manually examined the MS1 and MS2 spectra of all phosphopeptides that were preliminarily assessed as being changed in PKA-null cells. This resulted in a list of high confidence responses to vasopressin in the PKA-null cells (Table 1, https://hpcwebapps.cit.nih.gov/ESBL/Database/PKA-null/sites.html). Some example MS1 spectra corresponding to phospho-sites reported in Table 1 are shown in Supporting Figure S3.

Overall, these results suggest that (a) the major elements of vasopressin signaling are dependent on PKA, and (b) a smaller component of vasopressin signaling is independent of PKA.

3.4 | Baseline and dDAVP stimulated cAMP production in PKA-null cells

Vasopressin signaling is generally accepted to be cAMP-mediated. The marked decrease in the number of phosphorylation events in dDAVP-stimulated PKA-null cells may be related to the failure of cells to produce cAMP due to a dysfunctional V2R or by some other mechanism involving the $G_s\alpha$-adenylyl cyclase complex. To rule out such a possibility, we compared vasopressin-dependent cAMP-levels in PKA-intact versus PKA-null cells measured in the presence of the broad spectrum phosphodiesterase inhibitor IBMX (Figure 4). The PKA-null cells responded to dDAVP with a large increase in cAMP in the presence of IBMX. The surprising aspect of these data was a large increase in the baseline (vasopressin-independent) cAMP levels amounting to more than a 10-fold increase in PKA-null cells compared to PKA-intact cells (Figure 4A). It also shows an equivalent 10-fold increase of cAMP level in dDAVP-treated PKA-null cells when compared to dDAVP-treated PKA-intact cells. When the cells were not treated with IBMX, cAMP levels were still readily measurable, but values were not different between PKA-intact and PKA-null mpkCCD cells (Figure 4B). This indicates that under the conditions of the phosphoproteomic studies, cAMP production is likely to be markedly increased although high levels in the cells are not sustained due to rapid degradation by cyclic nucleotide phosphodiesterases. The measurements, however, do not rule out localized increases in cAMP levels. Overall, these measurements (a) confirmed the responsiveness of the PKA-null cells to vasopressin at the level of cAMP production, (b) suggest the presence of a PKA-controlled feedback inhibition of cAMP generation in PKA-intact cells.

3.5 | Vasopressin activates non-PKA basophilic kinases in PKA-null cells

Among the sites that were increased by dDAVP in PKA-null cells, there was a preponderance of sequences with a basic amino acid (eg R or K) in position −3 relative to the phosphorylated amino acid ($\chi^2 = 20.9$, $P = 5.00E\text{-}06$, versus all quantified monophosphopeptides). This implies that one or more basophilic protein kinases (AGC or CAMK group) were activated in response to dDAVP in the PKA-null cells. To narrow down the possibilities, we used prior transcriptomic data to identify basophilic kinases expressed in PKA-null mpkCCD cells,[9] augmenting this list with protein kinases found by nLC-MS/MS analysis in the present study. In Figure 4A, the circle shows the 47 basophilic kinases

TABLE 1 Vasopressin responsive phosphorylation sites in PKA-null cells

Accession	Gene symbol	Site(s)	Protein name	Centralized Sequence	Median Log_2(dDAVP/Vehicle)	$-log_{10}$ (P_{fp})
P59729	Rin3	S411	Ras and Rab interactor 3	GISRTAS*LNLPPQ	0.86	3.52
Q8R4H2	Arhgef12	S41	Rho guanine nucleotide exchange factor 12	KVERSSS*HDFDPT	0.79	3.28
Q8C1B1	Camsap2	S439	Calmodulin-regulated spectrin-associated protein 2	GIIRSVS*NEGLTL	0.75	3.16
Q9Z1E4	Gys1	S711[a]	Glycogen [starch] synthase, muscle	GSKRSNS*VDTGPS	0.70	2.98
P45481	Crebbp	S120	CREB-binding protein	LGAMGKS*PLNQGD	0.59	2.63
Q9D279	Misp	S364	Mitotic interactor and substrate of PLK1	GLQRSLS*SDCILS	0.59	2.67
Q9ERG2	Strn3	S202	Striatin-3	RSQRVRS*LLGLSN	0.58	2.95
Q3UHI0	Ccser2	S222	Serine-rich coiled-coil domain-containing protein 2	KMVRSQS*FSHSIQ	0.58	2.66
P19001	Krt19	S59	Keratin, type I cytoskeletal 19	VTSSSGS*YGGVRG	0.52	2.47
Q68ED7	Crtc1	S151	CREB-regulated transcription coactivator 1	SWRRTNS*DSALHQ	0.49	2.24
Q3TWF6	Wdr70	S641	WD repeat-containing protein 70	MFAQVES*DDEESK	0.49	2.75
A6H8H2	Dennd4c	S1321	DENN domain-containing protein 4C	YKDRSTS*LSALVR	0.48	1.98
Q9CY58	Serbp1	S203	Plasminogen activator inhibitor 1 RNA-binding protein	SGSDRSS*FSHYSG	0.48	2.18
Q8BG32	Psmd11	S14	26S proteasome non-ATPase regulatory subunit 11	EFQRAQS*LLSTDR	0.48	1.97
Q3B7Z2	Osbp	S377	Oxysterol-binding protein 1	GHKRTGS*NISGAS	0.39	2.48
Q60875	Arhgef2	S163	Rho guanine nucleotide exchange factor 2	GHFNDES*PLGLRQ	0.39	2.11
Q60875	Arhgef2	S151	Rho guanine nucleotide exchange factor 2	SLAKSVS*TTNIAG	0.39	2.31
Q9ESE1	Lrba	T1011	Lipopolysaccharide-responsive and beige-like anchor protein	SNTELQT*HDMSSD	0.37	2.44
Q6GYP7	Ralgapa1	S772	RalGTPase-activating protein subunit alpha-1	TRVRHFS*QSEDTG	0.33	2.62
Q9ESE1	Lrba	S1000	Lipopolysaccharide-responsive and beige-like anchor protein	SIGRASS*IDSASN	0.30	2.75
Q9Z1W9	Stk39	S383	STE20/SPS1-related proline-alanine-rich protein kinase	RRVPGSS*GHLHKT	0.29	2.60
P54310	Lipe	S559	Hormone-sensitive lipase	SMRRSVS*EAALAQ	0.25	3.34
P99027	Rplp2	S79	60S acidic ribosomal protein P2	VSAAPGS*AAPAAG	−0.18	1.33
Q8BTM8	Flna	S968	Filamin-A	SVGVSPS*LDLSKI	−0.20	2.98
Q9JKB3	Ybx3	S52	Y-box-binding protein 3	AALLAGS*PGGDAA	−0.20	2.75
Q62074	Prkci	T411	Protein kinase C iota type	PGDTTST*FCGTPN	−0.34	2.39
Q62074	Prkci	T415	Protein kinase C iota type	TSTFCGT*PNYIAP	−0.35	2.32
Q9D1C9	Rrp7a	S99	Ribosomal RNA-processing protein 7 homolog A	KPDLAES*PTEPKS	−0.35	2.12
Q8C0T5	Sipa1l1	S1626	Signal-induced proliferation-associated 1-like protein 1	HGEFSAS*DSSLTD	−0.45	1.99
Q9Z2H5	Epb41l1	S378	Band 4.1-like protein 1	TFFRLVS*PEPPPK	−0.45	2.39
P99027	Rplp2	S86	60S acidic ribosomal protein P2	AAPAAGS*APAAAE	−0.59	3.65
P39447	Tjp1	S280	Tight junction protein ZO-1	LSDSIHS*ANASER	−0.65	2.25
Q3UHX2	Pdap1	S60[a]	28 kDa heat- and acid-stable phosphoprotein	EKKSLDS*DESEDE	−0.83	1.25
P11276	Fn1	S285[a]	Fibronectin	ASAGSGS*FTDVRT	−0.84	3.67
Q99J36	Thumpd1	S88	THUMP domain-containing protein 1	DQQPSGS*EGEDDD	−0.94	4.60
P09405	Ncl	S145	Nucleolin	NAKKEDS*DEDEDE	−1.64	16.00
Q3THK3	Gtf2f1	S311	General transcription factor IIF subunit 1	SESSEES*EEEKPP	−2.46	15.60

[a]These sites have redundant quantification evidence showing similar changes (eg PKA-null and PKA-intact cells, site containing peptides with or without missed cleavage, and HCD-EThcD pairs). The MS1 spectra of monophosphopeptides containing these sites can be found in Supporting Figure S3. Eleven of the increased phosphorylation sites are putative SNF1-subfamily targets based on the presence of an (R/K)-(T/S)-X-p(S/T) motif with nonpolar amino acid in position −5 and/or position +4 relative to the phosphorylated amino acid (underlined amino acids).

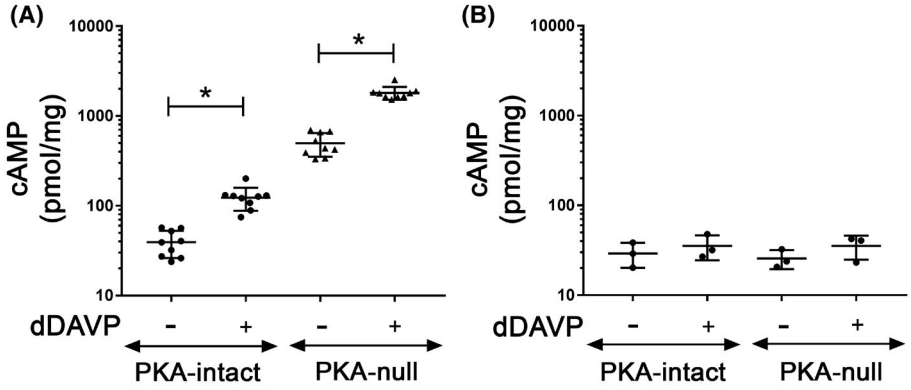

FIGURE 4 Effect of dDAVP on cAMP generation in PKA-intact and PKA-null cells. The experiment was performed (A) in the presence or (B) in the absence of IBMX. The measured cAMP values in pmol/mL were normalized with the protein concentration of the respective samples. Data were presented as mean ± SD. A two-tailed independent samples *t*-test was used. n ≥ 3; **P* < .05; SD = standard deviation

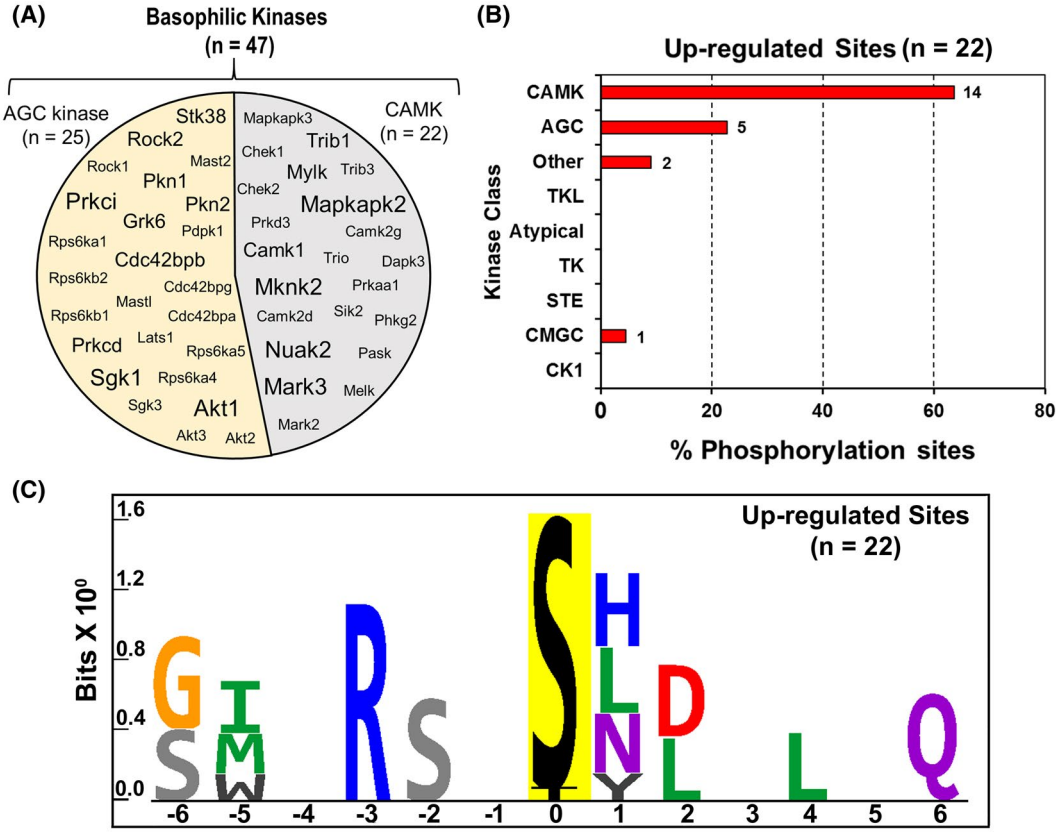

FIGURE 5 A, The circle contains gene symbols of 47 basophilic kinases expressed in PKA-null cells. The font-size corresponds to their expression at the RNA level as determined earlier by Isobe et al.[9] B, Histogram to predict relative frequency of various kinase classes upstream of altered phospho-sites in dDAVP treated PKA-null cells. A total of 22 elevated phospho-sites were analyzed using GPS 3.0 to predict the class of individual kinases. A frequency distribution analysis was performed to determine the % of phospho-sites (x-axis) that belong to certain class of kinase (y-axis). CAMK (14/22, 63%) were the most frequently predicted kinase class among upregulated sites in PKA-null cells. C, Sequence logo for the up-regulated phosphorylation sites in dDAVP treated PKA-null cells. PTM-Logo was used for motif analysis. The background contains all unique and mono-phosphorylated peptides

(out of 126 basophilic kinases in the mouse kinome) that are expressed at both transcript and protein levels in PKA-null cells. This list contains 25 kinases from the AGC group and 22 kinases from the CAMK group. The CAMK group of kinases was predicted to account for a majority of (14/22, 64%) elevated phospho-sites in PKA-null cells (Figure 5B) based on the *Group-based Prediction System* (GPS 3.0).[13] This program uses machine-learning approaches to optimize the match between individual phosphorylation sites and kinase preference motifs across the kinome to identify the kinase

group, kinase family, kinase subfamily and individual kinase level matches. Additional analysis revealed preferences for serine or threonine in position −2 (χ^2 = 14.4, P = 1.45E-04), hydrophobic amino acids (isoleucine, methionine and tryptophan) in position −5 (χ^2 = 23.4, P = 1.00E-06) and in position +4 (glycine, leucine, isoleucine and valine, χ^2 = 7.4, P = 6.41E-03). Figure 4C shows the preferred motif that was created using *PTM-Logo* [12] from the list of increased phospho-sites. Overall, among the increased phospho-sites there were eleven with either of the two motifs: ([I/M/W]-X-[R/K]-[S/T]-X-p[**S/T**], or [R/K]-[S/T]-X-p[**S/T**]-X-X-X-[G/L/I/V]), including some with hydrophobic amino acids in both −5 and +4 position (Table 1). These motifs are not a general feature of the CAMK group, but correspond to the CAMK branch known as the AMPK-related kinase subfamily (or SNF1-subfamily), which includes the AMP-activated protein kinases Prkaa1 and Prkaa2, the MAP/microtubule affinity-regulating kinases Mark1 through Mark4, the salt-inducible kinases Sik1 through Sik3, the SNF1-like kinases Nuak1 and Nuak2, the BR serine/threonine kinases Brsk1 and Brsk2, and the maternal embryonic leucine zipper kinase Melk.[18] Further, at least three of the increased phosphorylation sites in Table 1 have been experimentally characterized in other cell types and linked to kinases from the SNF1-subfamily. These sites are: S151 of Arhgef2 (Rho guanine nucleotide exchange factor 2, upstream kinase: Mark3[19]); S151 of Crtc1 (CREB-regulated transcription coactivator 1, upstream kinase: Sik2 or Prkaa1[20]); and S559 of Lipe (Hormone-sensitive lipase, upstream kinase: Prkaa1[21]). Together, these results indicate probable activation of one or more members of the SNF1 (AMPK-related) kinase subfamily in PKA-null cells following dDAVP stimulation. It is noteworthy that two other protein kinases with no obvious relationship to AMPK/SNF1-subfamily kinases undergo changes at activity-altering phosphorylation sites in response to vasopressin in the PKA-null cells. These kinases are Stk39 (SPAK, at S383) which is increased, and Prkci (PKC-iota, at T411 and T415) which shows decreased phosphorylation.

3.6 | In vitro phosphorylation by recombinant SNF1-subfamily protein kinases

Several SNF1-subfamily protein kinases are expressed in mpkCCD cells, namely Prkaa1 (AMPKα1), Sik2, Mark2, Mark3, Nuak2 and Melk (Figure 5A). We asked which among these are responsible for increased phosphorylation in PKA-null cells following dDAVP treatment. First, we focused on AMPK as it is the major and most well-studied member of SNF1-subfamily of basophilic kinase. Phosphorylation of conserved T172 present within the activation loop of the α-subunit kinase domain of AMPKα2 (Prkaa2, analogous to T183 of Prkaa1/AMPKα1) is known to activate this kinase.[18] However, immunoblot results do not show an increase in the phosphorylation on T172 of AMPKα following dDAVP treatment in PKA-null or intact cells when compared to vehicle-treated cells (Figure 6). AMPK can also be activated allosterically by AMP that may not necessarily need a pre-phosphorylation of AMPKα in its activation loop.[18] To test this possibility, we designed an in vitro phosphorylation assay with custom-made human recombinant AMPKα that is not phosphorylated at its activation loop. AMPK heterotrimers consist of catalytic α subunit (α1 or α2) along with a scaffolding β (β1 or β2) subunit and a regulatory γ (either γ1, or γ2, or γ3) subunit. Here, we used three different versions of heterotrimeric AMPK; namely AMPKα1β1γ1, AMPKα1β2γ1, and AMPKα2β2γ1.

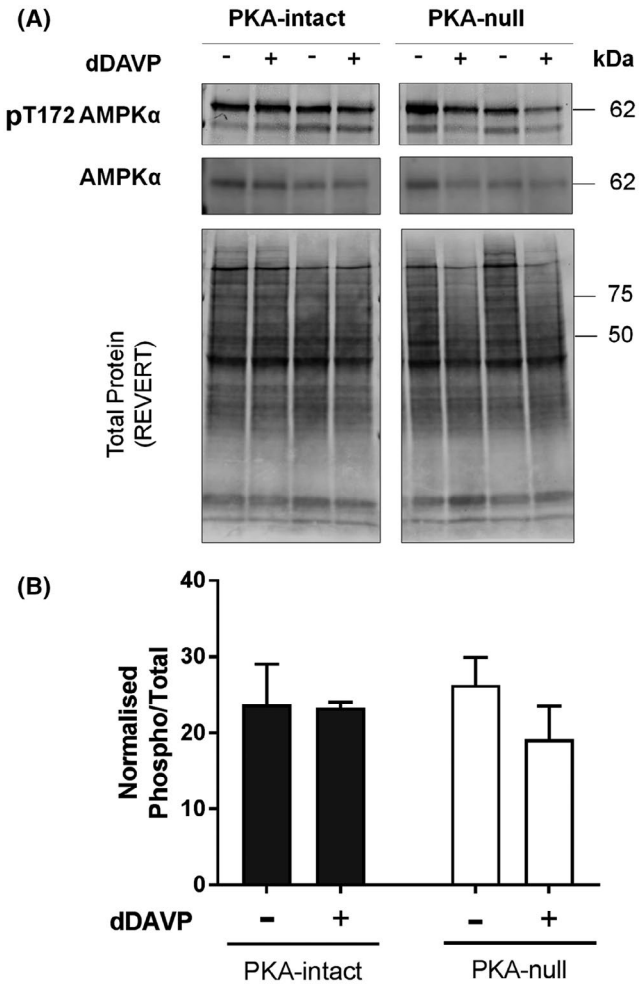

FIGURE 6 Immunoblot analysis to detect differential phosphorylation at the active site of AMPKα. A, AMPKα and pT172-AMPKα immunoblot from dDAVP- and vehicle-treated PKA-intact and PKA-null cells. The gels were stained with REVERT (Li Cor) stain to check equal loading among different samples. B, Bar chart of normalized immuno-reactivities (mean ± SEM in arbitrary units) of pT172 AMPKα. Unpaired *t*-test was used to determine significant difference between dDAVP and vehicle-treated samples. dDAVP did not cause a significant difference in phosphorylation of T172 of AMPKα in PKA-intact or PKA-null cells. *P < .05

Centralized 13-mer synthetic peptides around the elevated phosphorylation sites of Arhgef2 (S151), Crtc1 (S151) and Lipe (S559) protein with a matching SNF1 motif were used as substrates for this in vitro assay. Because it seemed possible that cAMP could substitute for AMP as an allosteric activator of AMPK, we tested varying concentrations of cAMP (10-1000 μM) in addition to AMP (10-100 μM) in the reaction mixture. PRM-MS was used to measure phosphopeptides and to quantify site-specific phosphorylation using a diagnostic transition ion or neutral loss ion as described in Section 2 (Supporting Table S2). Standard AMPK/Sik2 substrates AMARA and SAMS-tide were also included as positive controls. As shown in Figure 7A, increasing concentrations of cAMP (10-1000 μM) were unable to increase the phosphorylation of any of the above-mentioned three sites or the target sites in standard peptides. Instead, cAMP appears to inhibit phosphorylation at higher concentrations. In contrast, AMP increased phosphorylation of all three sites at the tested concentrations that were elevated in mpkCCD cells in response to dDAVP (Figure 7B). Standard peptides also showed similar trends. Thus, AMPK is a candidate for a role in vasopressin-induced phosphorylation changes in PKA-null mpkCCD cells, but it cannot be allosterically activated by cAMP.

3.7 | Non-AMPK members of SNF1-subfamily can phosphorylate selected sites of Arhgef2, Crtc1, and lipe

To search for potential alternate mechanisms behind the elevation of phospho-sites with the SNF1 recognition motif, we extended the in vitro phosphorylation assay on the same set of target substrates to include additional members of the SNF1-subfamily of kinases, namely Mark3, Nuak2, Melk, and Sik2. The choice of these enzymes was driven by the objective to include multiple kinases from different branches of the SNF1-subfamily that are expressed in PKA-null cells. Our results show that under in vitro conditions, Mark3, Sik2, Nuak2, and Melk can all phosphorylate the sites in Arhgef2, Crtc1, and Lipe (Figure 8) and that the activity of these enzymes was not increased by AMP addition (Figure 9).

4 | DISCUSSION

We used quantitative phosphoproteomics to show that V2R-mediated vasopressin signaling in cultured collecting duct cells is predominantly PKA-dependent. In addition, there is a smaller component that is PKA-independent, likely involving activation of one or more members of the AMPK/SNF1-subfamily of the CAMK-like family of kinases. Among the PKA-independent phosphorylation targets that were detected were three known targets of SNF1-subfamily kinases, namely Arhgef2 (S151), Crtc1 (S151), and Lipe (S559).[19-21] Further, we show that the vasopressin-induced increase in phosphorylation of AQP2 at Ser256 can occur in the absence of PKA, although the specific kinase involved was not identified.

4.1 | Prior evidence for PKA-independent vasopressin responses in collecting duct

A number of prior studies in collecting duct cells have provided evidence for cAMP- or PKA- independent effects of

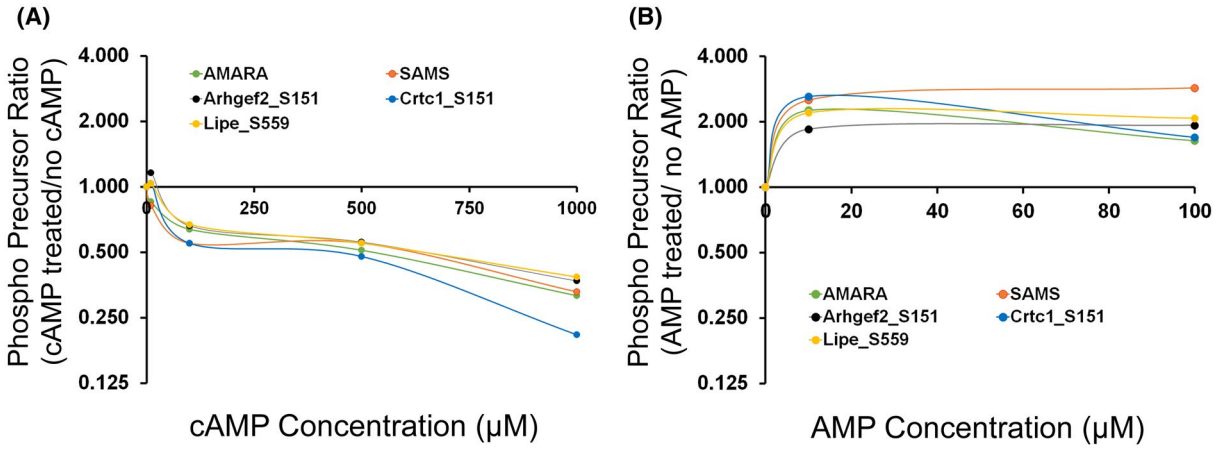

FIGURE 7 PRM-MS measurement of mono-phosphorylated form of 13-mer synthetic peptides centralized around S151 of Arhgef2, S151 of Crtc1 and S559 of Lipe. Human recombinant AMPK (eg AMPKα2β2γ1) that was not phosphorylated at its active site, was used for the in vitro phosphorylation reaction. AMARA and SAMS were used as standard peptide substrates for AMPK phosphorylation. A, Effect of increasing concentrations of cAMP (0, 10, 100, 500, 1000 μM) on AMPK-induced phosphorylation. B, Effect of increasing concentrations of AMP (0, 10, 100 μM) on AMPK-induced phosphorylation. X-axis indicates the ratio of chromatographic area of phosphorylated peptides (based on precursor ion chromatogram area) following incubation with various concentrations of (A) cAMP (B) AMP when compared to (A) "no cAMP" or (B) "no AMP" (0 μM). An x-axis value of 1.0 indicates no change

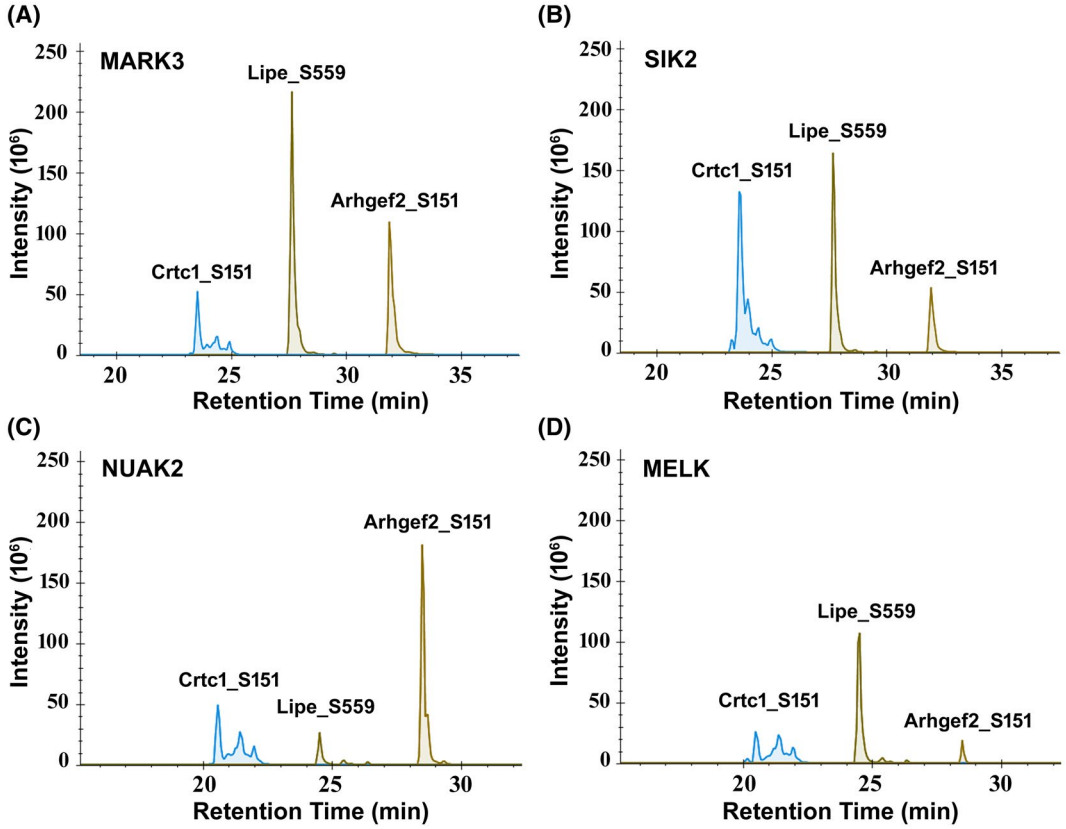

FIGURE 8 Precursor ion chromatogram of phosphorylated 13-mer synthetic peptides centralized around S151 of Arhgef2, S151 of Crtc1 and S559 of Lipe. The synthetic peptides were phosphorylated following an in vitro phosphorylation reaction in presence of various human recombinant SNF1-subfamily of kinases; (A) MARK3, (B) SIK2, (C) NUAK2, (D) MELK. The phosphorylation occurs predominantly at the target site of the respective peptides as determined by the chromatogram area of site-specific product ions. All SNF1-subfamily enzymes can phosphorylate the three selected phosphorylation sites on Arhgef2 (S151), Crtc1 (S151) and Lipe (S559) to different extent under in vitro condition

vasopressin. Olesen et al[22] have questioned the role of cAMP in vasopressin-mediated trafficking to the plasma membrane, based on differences in the time courses of intracellular cAMP changes and immunochemical detection of AQP2 redistribution in collecting duct cells. Nickols et al[23] found that V2-receptor mediated mobilization of intracellular Ca^{2+} was blocked by mutation of a calmodulin-binding site in the COOH-terminal tail of the V2 receptor, without affecting cAMP production. The presence of cAMP-independent mobilization of intracellular Ca^{2+} in collecting duct cells was also supported by Naruse,[24] Star et al,[25] and Champigneulle et al[26] On the contrary, the finding that vasopressin-mediated Ca^{2+} mobilization was replicated in collecting ducts in response to exposure to cAMP analogs suggests that Ca^{2+} mobilization is at least in part cAMP dependent.[27] Beyond this, Yip[28] has provided evidence that cAMP-mediated Ca^{2+} mobilization, and concomitant AQP2 trafficking to the plasma membrane, could be the result of cAMP activation of the Rap1 guanine-nucleotide exchange factor, Epac1 (Rapgef3) and not PKA. Another study provided evidence for a role for Epac1, but not PKA, in the effect of long-term exposure to vasopressin to increase *Aqp2* gene transcription.[29] Activation of Epac1 is predicted to activate Rap1 through its guanine-nucleotide exchange factor (GEF) activity. Rap1, among other functions, competes with Ras to reduce MAP kinase signaling.[30] However, there was no evidence in the present study of altered phosphorylation of any MAP kinase in response to vasopressin in the PKA-null cells. Beyond this, in our prior study, deletion of both PKA catalytic genes abrogated the effect of vasopressin to stimulate *Aqp2* gene transcription and AQP2 trafficking, and these effects were rescued by transfection with PKA,[9] strongly supporting a central role for PKA in both actions of vasopressin.

4.2 | Possible mechanisms of accelerated cAMP production in PKA-null cells

A potentially important new finding in this paper is the observation that IBMX-dependent cAMP levels are around 10-fold higher in PKA-null cells than in PKA-intact cells. Since the difference in cAMP levels between PKA-null cells and PKA-intact cells was not seen in the absence of the phosphodiesterase inhibitor IBMX, we conclude that PKA-null

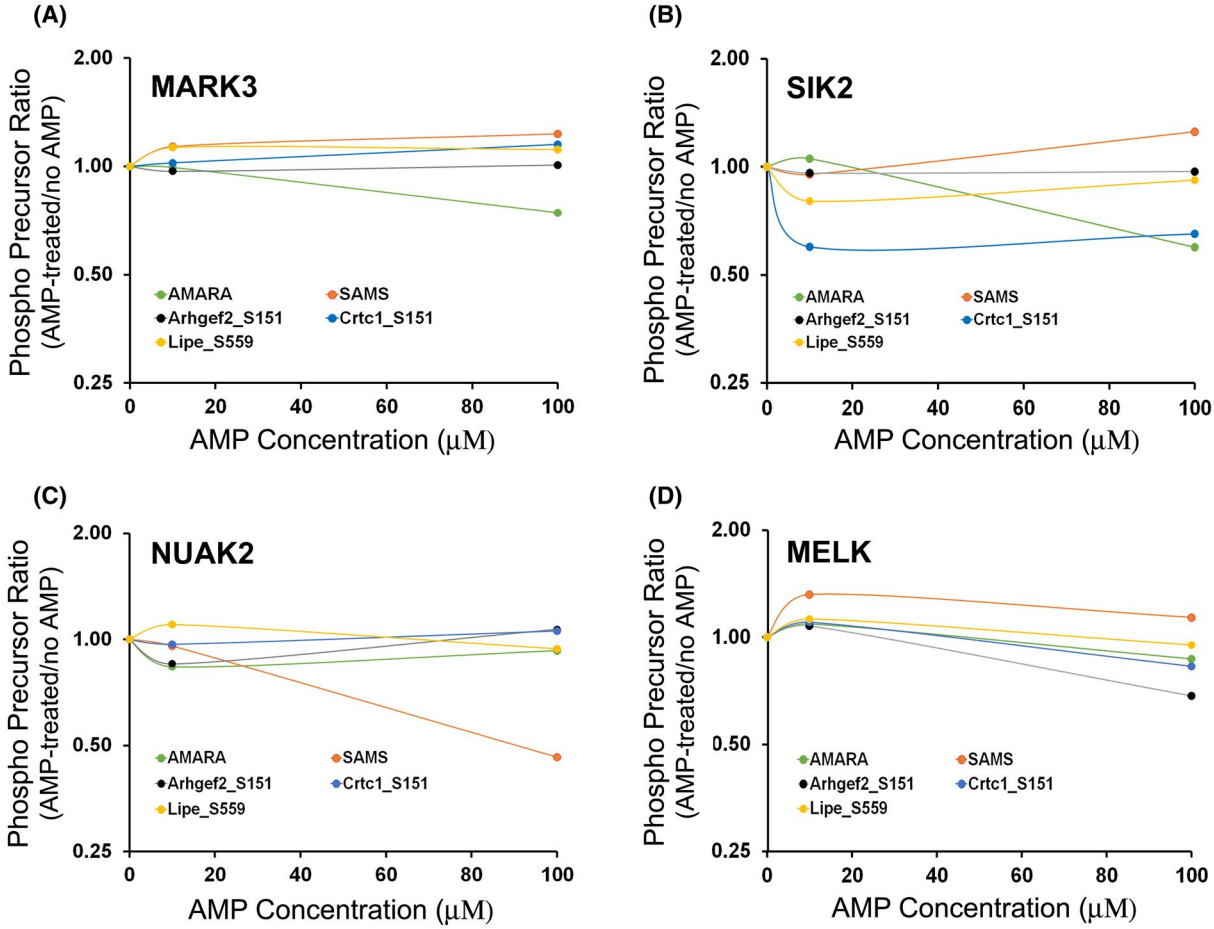

FIGURE 9 Effect of increasing concentration of AMP on the phosphorylation of 13-mer synthetic peptides centralized around S151 of Arhgef2, S151 of Crtc1 and S559 of Lipe in presence of various SNF1-subfamily protein kinases. Human recombinant (A) MARK3, (B) SIK2, (C) NUAK2, (D) MELK were used for the in vitro phosphorylation reaction. PRM-MS assay was used to measure the chromatogram area of phosphorylated peptide precursors. X-axis indicates the ratio of chromatogram area of phosphorylated peptides (based on precursor mass) following incubation with various concentrations of AMP (10, 100 μM) when compared to "no AMP" (0 μM). An x-axis value of 1.0 indicates no change. AMARA and SAMS were included as control peptides

cells likely have accelerated cAMP production. The most direct interpretation of this finding is that there may be a PKA-dependent feedback mechanism at the level of the V2R-adenylyl cyclase pathway that is interrupted with PKA deletion. There are several possibilities that could account for this feedback inhibition based on the various components of the coupling mechanism connecting receptor occupation and cAMP production, namely the V2R receptor (Avpr2), the heterotrimeric G-protein stimulatory alpha subunit $G_s\alpha$ (Gnas) or its inhibitory counterparts, the RGS protein Rgs3 (a GTPase activating protein), and adenylyl cyclase 6 (Adcy6). Among these, only Rgs3 showed a change in phosphorylation in response to dDAVP in the PKA-intact cells, viz. an increase in phosphorylation at a basophilic site (S686), although the effect of this modification on its activity is currently unknown based on the data on *PhosphoSitePlus*. In general, protein function can be regulated by processes other than phosphorylation and it will require a systematic examination of multiple competing hypotheses to identify the feedback mechanism responsible for the high cAMP levels in the PKA-null cells.

4.3 | Possible mechanisms of vasopressin signaling in the absence of PKA

The mechanism by which vasopressin activates downstream signaling in the absence of PKA has not yet been identified. As vasopressin signals through the $G_\alpha s$-coupled GPCR V2R, it is likely that the activation involves cAMP. We propose four possible mechanisms of PKA-independent cAMP effects: (a) cAMP could be working through effectors other than PKA, eg Rapgef3 (Epac1); (b) cAMP could act allosterically to increase AMPK activity, mimicking AMP; (c) high AMP concentration could be achieved locally in the cell due to increased production and degradation of cAMP that could activate AMPK locally; and (d) high cAMP could directly activate other kinases

such as Protein Kinase G. The first possibility seemed to be a viable choice because of observations in the literature that RapGEF3/Epac1 can activate the protein kinase Lkb1 (Stk11), which activates AMPK through active site phosphorylation.[31] However, immunoblotting for active site phosphorylation of AMPKα failed to show any tendency toward an increase in phosphorylation, ruling out this specific mechanism (Figure 6). The second possibility was seemingly ruled out by in vitro phosphorylation assays showing that cAMP, even at very high concentrations, inhibits rather than activates AMPK (Figure 7A). The third possibility was supported in part by the results of in vitro phosphorylation assays that confirm that AMP can indeed enhance the ability of AMPK to phosphorylate three specific targets increased by vasopressin in PKA-null cells (Figure 7B). In addition, we found that several other SNF1-subfamily protein kinases can also target the regulated phosphorylation sites in vitro (Figure 8). Consistent with the fourth possibility, cGMP-activated kinases (Protein Kinase G) have been shown to be activated by high levels of cAMP, similar to those measured in PKA-null cells in the present study.[32,33] Prior studies have found that AMPK can be activated by nitric oxide working through cGMP [34,35] pointing to a role for Protein Kinase G in the regulation of AMPK. It is not clear whether activation of Protein Kinase G can cause activation of other SNF1-subfamily kinases, however.

4.4 | Downstream effects of SPAK, atypical PKC, and SNF1-subfamily protein kinases in vasopressin action

The phosphoproteomics data in this study indicate that, in the absence of PKA, vasopressin activates the protein kinase SPAK (Stk39) and one or more members of the SNF1 (AMPK-related) kinase subfamily. It also decreases activation of an atypical protein kinase C (Prkci) through a decrease in active site phosphorylation (T411). SPAK has previously been implicated in the regulation of blood pressure and NaCl balance through effects in the distal nephron.[36] SPAK phosphorylation was increased by vasopressin in PKA-null cells at a site in its regulatory domain (S383), a known target of the "With-No-K" protein kinase WNK4.[37] Vasopressin activates the thiazide-sensitive Na-Cl cotransporter in association with increased SPAK phosphorylation [38] and the regulation is ablated by SPAK deletion,[39] indicating that the vasopressin effect on NaCl transport is dependent on SPAK activation. Although SPAK has been best characterized in non-AQP2 expressing cells, it has been found to be strongly expressed in collecting duct principal cells,[40] although a specific role in AQP2 regulation has not yet been explicitly assigned.

Activation of one or more SNF1-subfamily kinases by vasopressin in PKA-null mpkCCD cells may have implications with regard to the regulation of AQP2. Prior studies implicated AMPK in the regulation of AQP2 trafficking[41,42] and osmotic water transport[41,43] in the renal collecting duct. Furthermore, data from a cultured collecting duct cell line, MDCK, provided strong evidence for a central role of another SNF1-subfamily kinase, viz. Mark2 (Par-1), in the regulation of collecting duct cell polarity and vesicular trafficking.[44-54] PKC-iota is an "atypical" protein kinase C, ie it is calcium- and diacylglycerol-independent, that plays an important role in creating and maintaining epithelial polarity.[55]

A key finding was that, in both PKA-intact and PKA-null cells, vasopressin increased phosphorylation of AQP2 at a key residue, S256, which is believed to be critical to AQP2 trafficking to the plasma membrane.[56] Thus, some non-PKA protein kinase can phosphorylate S256 of AQP2. A Bayesian analysis of AQP2 phosphorylation identified the protein kinases (among the 523 protein kinases in the mouse genome) that are most likely to phosphorylate S256, based on integration of multiple data types.[57] The top-ranked kinases included several SNF1-subfamily kinases including Mark2, Mark3, and Nuak2. It also included non-SNF1-subfamily kinases, Prkci and Protein Kinase G (Prkg2), but not SPAK. Evidence for a role for Protein Kinase G has previously been presented by Bouley and colleagues.[58] Other studies have also proposed S256 phosphorylation by other non-PKA protein kinases including AKT,[59] casein kinase,[60] and protein kinase C-δ (PKCδ),[59] none of which derive support from the present study.

An additional important question is whether the activation of one or more SNF1-subfamily kinases seen in PKA-null cells also occur in PKA-intact cells. In the present study, there are two sites (S711 of Gys1 and S377 of Osbp) that responded to V2R stimulation with an increase in phosphorylation in both PKA-null and PKA-intact cells (Supporting Table S3). Prats et al had showed that PKA phosphorylates human muscle Gys1 on S710 (analogous to S711 in mouse) following exhausting exercise that alters its intracellular distribution.[61] Mohammadi et al reported S381 of rabbit Osbp (analogous to S377 in mouse) as a cholesterol-sensitive phosphorylation site.[62] Notably, in PKA-intact cells, no changes in phosphorylation in Arhgef2 at S151, Crtc1 at S151 or Lipe at S559 were observed. In our previous study in PKA-intact cells, vasopressin exposure was shown to trigger Crtc1 translocation into the nucleus,[9] although a change in S151 phosphorylation was not tested. Overall, majority of the putative SNF1-subfamily kinase targets that increased in PKA-null cells due to V2R stimulation, remained unchanged in PKA-intact cells. We, therefore, speculate that the activation of SNF1-subfamily kinases may be dependent on the very high cAMP production rate in the PKA-null cells and may not be a general feature of PKA signaling.

4.5 | Data sharing

Although this paper focuses on signaling processes related to the action of vasopressin to regulate water transport in the kidney, the experimental system that we used in this study can be viewed as a model of $G_s\alpha$-coupled GPCR signaling in general. To facilitate the use of the data in the future, we have provided the curated datasets in the form of two publically accessible databases (PKA-null and PKA-intact). In general, our own analysis only "scratched the surface" regarding the bioinformatic analysis of these data and hope that the provision of these publicly accessible data resources will facilitate its utilization.

ACKNOWLEDGEMENTS

This work was funded by the Division of Intramural Research, National Heart, Lung and Blood Institute (Projects ZIA-HL-001285 and ZIA-HL-006129, to M. A. Knepper). We thank Angel Aponte, Guanghui Wang and Marjan Gucek of the NHLBI Proteomics Core Facility for mass spectrometry assistance. We thank Kiyoshi Isobe, Hyun Jun Jung, Lihe Chen, and Anika Kao for helpful discussions.

CONFLICT OF INTEREST

No conflicts of interest, financial or otherwise, are declared by the author(s).

AUTHOR CONTRIBUTIONS

MAK, AD, and VR designed research; AD performed all experiments; AD, MAK, CRY, and VR analyzed the data:, AD, KL, CRY did webpage generation and skyline data analysis; MMR provided advice regarding the targeted mass spectrometry experiments; CLC provided useful discussion of data interpretation; AD and MAK wrote the paper. All authors edited and approved the final version of the manuscript.

DATA AVAILABILITY STATEMENT

Mass spectrometer generated raw (.raw) and analysis (.msf) files for SILAC experiment have been uploaded to the ProteomeXchange Consortium via the PRIDE partner repository with the dataset identifier PXD015719. These data are accessible at www.ebi.ac.uk/pride/archive/. The curated files have been made available through publicly available webpages: (a) PKA-null dataset: https://hpcwebapps.cit.nih.gov/ESBL/Database/PKA-null/index.html; (b) PKA-intact dataset: https://hpcwebapps.cit.nih.gov/ESBL/Database/PKA-Intact/index.html.

REFERENCES

1. Knepper MA, Kwon T-H, Nielsen S. Molecular physiology of water balance. *N Engl J Med*. 2015;372:1349-1358.
2. Nielsen S, Frokiaer J, Marples D, Kwon TH, Agre P, Knepper MA. Aquaporins in the kidney: from molecules to medicine. *Physiol Rev*. 2002;82:205-244.
3. Nielsen S, Chou CL, Marples D, Christensen EI, Kishore BK, Knepper MA. Vasopressin increases water permeability of kidney collecting duct by inducing translocation of aquaporin-CD water channels to plasma membrane. *Proc Natl Acad Sci U S A*. 1995;92:1013-1017.
4. Brown D. The ins and outs of aquaporin-2 trafficking. *Am J Physiol Renal Physiol*. 2003;284:F893-F901.
5. Matsumura Y, Uchida S, Rai T, Sasaki S, Marumo F. Transcriptional regulation of aquaporin-2 water channel gene by cAMP. *J Am Soc Nephrol*. 1997;8:861-867.
6. Hasler U, Leroy V, Martin PY, Feraille E. Aquaporin-2 abundance in the renal collecting duct: new insights from cultured cell models. *Am J Physiol Renal Physiol*. 2009;297:F10-18.
7. Sandoval PC, Claxton JS, Lee JW, Saeed F, Hoffert JD, Knepper MA. Systems-level analysis reveals selective regulation of Aqp2 gene expression by vasopressin. *Sci Rep*. 2016;6:34863.
8. Uchida S, Sasaki S, Fushimi K, Marumo F. Isolation of human aquaporin-CD gene. *J Biol Chem*. 1994;269:23451-23455.
9. Isobe K, Jung HJ, Yang CR, et al. Systems-level identification of PKA-dependent signaling in epithelial cells. *Proc Natl Acad Sci U S A*. 2017;114:E8875-E8884.
10. Loo CS, Chen CW, Wang PJ, et al. Quantitative apical membrane proteomics reveals vasopressin-induced actin dynamics in collecting duct cells. *Proc Natl Acad Sci U S A*. 2013;110:17119-17124.
11. Schenk LK, Bolger SJ, Luginbuhl K, et al. Quantitative proteomics identifies vasopressin-responsive nuclear proteins in collecting duct cells. *J Am Soc Nephrol*. 2012;23:1008-1018.
12. Saethang T, Hodge K, Yang CR, et al. PTM-Logo: a program for generation of sequence logos based on position-specific background amino-acid probabilities. *Bioinformatics*. 2019;35:5313-5314.
13. Xue Y, Ren J, Gao X, Jin C, Wen L, Yao X. GPS 2.0, a tool to predict kinase-specific phosphorylation sites in hierarchy. *Mol Cell Proteomics*. 2008;7:1598-1608.
14. MacLean B, Tomazela DM, Shulman N, et al. Skyline: an open source document editor for creating and analyzing targeted proteomics experiments. *Bioinformatics*. 2010;26:966-968.
15. Dephoure N, Gould KL, Gygi SP, Kellogg DR. Mapping and analysis of phosphorylation sites: a quick guide for cell biologists. *Mol Boil Cell*. 2013;24:535-542.
16. Yu MJ, Miller RL, Uawithya P, et al. Systems-level analysis of cell-specific AQP2 gene expression in renal collecting duct. *Proc Natl Acad Sci U S A*. 2009;106:2441-2446.
17. Nishimoto G, Zelenina M, Li D, et al. Arginine vasopressin stimulates phosphorylation of aquaporin-2 in rat renal tissue. *Am J Physiol Renal Physiol*. 1999;276:F254-F259.
18. Hardie DG, Schaffer BE, Brunet A. AMPK: an energy-sensing pathway with multiple inputs and outputs. *Trends Cell Biol*. 2016;26:190-201.
19. Sandi MJ, Marshall CB, Balan M, et al. MARK3-mediated phosphorylation of ARHGEF2 couples microtubules to the actin cytoskeleton to establish cell polarity. *Sci Signaling*. 2017;10(503):eaan3286.
20. Altarejos JY, Montminy M. CREB and the CRTC co-activators: sensors for hormonal and metabolic signals. *Nat Rev Mol Cell Biol*. 2011;12:141-151.

21. Donsmark M, Langfort J, Holm C, Ploug T, Galbo H. Contractions induce phosphorylation of the AMPK site Ser565 in hormone-sensitive lipase in muscle. *Biochem Biophys Res Commun*. 2004;316:867-871.
22. Olesen ET, Moeller HB, Assentoft M, MacAulay N, Fenton RA. The vasopressin type 2 receptor and prostaglandin receptors EP2 and EP4 can increase aquaporin-2 plasma membrane targeting through a cAMP-independent pathway. *Am J Physiol Renal Physiol*. 2016;311:F935-F944.
23. Nickols HH, Shah VN, Chazin WJ, Limbird LE. Calmodulin interacts with the V2 vasopressin receptor: elimination of binding to the C terminus also eliminates arginine vasopressin-stimulated elevation of intracellular calcium. *J Biol Chem*. 2004;279:46969-46980.
24. Naruse M. Arginine vasopressin increases intracellular calcium ion concentration in isolated mouse collecting tubule cells: distinct mechanism of action through V2 receptor, but independent of adenylate cyclase activation. *Nihon Jinzo Gakkai Shi*. 1992;34:337-347.
25. Star RA, Nonoguchi H, Balaban R, Knepper MA. Calcium and cyclic adenosine monophosphate as second messengers for vasopressin in the rat inner medullary collecting duct. *J Clin Invest*. 1988;81:1879-1888.
26. Champigneulle A, Siga E, Vassent G, Imbert-Teboul M. V2-like vasopressin receptor mobilizes intracellular Ca^{2+} in rat medullary collecting tubules. *Am J Physiol Renal Physiol*. 1993;265:F35-45.
27. Chou CL, Yip KP, Michea L, et al. Regulation of aquaporin-2 trafficking by vasopressin in the renal collecting duct. Roles of ryanodine-sensitive Ca^{2+} stores and calmodulin. *J Biol Chem*. 2000;275:36839-36846.
28. Yip KP. Epac-mediated Ca^{2+} mobilization and exocytosis in inner medullary collecting duct. *Am J Physiol Renal Physiol*. 2006;291:F882-890.
29. Kortenoeven ML, Trimpert C, van den Brand M, Li Y, Wetzels JF, Deen PM. In mpkCCD cells, long-term regulation of aquaporin-2 by vasopressin occurs independent of protein kinase A and CREB but may involve Epac. *Am J Physiol Renal Physiol*. 2012;302:F1395-1401.
30. Zwartkruis FJ, Bos JL. Ras and Rap1: two highly related small GTPases with distinct function. *Exp Cell Res*. 1999;253:157-165.
31. Fu D, Wakabayashi Y, Lippincott-Schwartz J, Arias IM. Bile acid stimulates hepatocyte polarization through a cAMP-Epac-MEK-LKB1-AMPK pathway. *Proc Natl Acad Sci U S A*. 2011;108:1403-1408.
32. Lorenz R, Bertinetti D, Herberg FW. cAMP-Dependent Protein Kinase and cGMP-Dependent Protein Kinase as Cyclic Nucleotide Effectors. *Handb Exp Pharmacol*. 2017;238:105-122.
33. Kim JJ, Casteel DE, Huang G, et al. Co-crystal structures of PKG Ibeta (92–227) with cGMP and cAMP reveal the molecular details of cyclic-nucleotide binding. *PloS one*. 2011;6:e18413.
34. Deshmukh AS, Long YC, de Castro Barbosa T, et al. Nitric oxide increases cyclic GMP levels, AMP-activated protein kinase (AMPK)alpha1-specific activity and glucose transport in human skeletal muscle. *Diabetologia*. 2010;53:1142-1150.
35. Murphy BA, Fakira KA, Song Z, Beuve A, Routh VH. AMP-activated protein kinase and nitric oxide regulate the glucose sensitivity of ventromedial hypothalamic glucose-inhibited neurons. *Am J Physiol Cell Physiol*. 2009;297:C750-758.
36. Richardson C, Alessi DR. The regulation of salt transport and blood pressure by the WNK-SPAK/OSR1 signalling pathway. *J Cell Sci*. 2008;121:3293-3304.
37. Gagnon KB, Delpire E. On the substrate recognition and negative regulation of SPAK, a kinase modulating Na^+-K^+-$2Cl^-$ cotransport activity. *Am J Physiol Cell Physiol*. 2010;299:C614-C120.
38. Pedersen NB, Hofmeister MV, Rosenbaek LL, Nielsen J, Fenton RA. Vasopressin induces phosphorylation of the thiazide-sensitive sodium chloride cotransporter in the distal convoluted tubule. *Kidney Int*. 2010;78:160-169.
39. Saritas T, Borschewski A, McCormick JA, et al. SPAK differentially mediates vasopressin effects on sodium cotransporters. *J Am Soc Nephrol*. 2013;24:407-418.
40. Chen L, Lee JW, Chou CL, et al. Transcriptomes of major renal collecting duct cell types in mouse identified by single-cell RNA-seq. *Proc Natl Acad Sci U S A*. 2017;114:E9989-e9998.
41. Klein JD, Wang Y, Blount MA, et al. Metformin, an AMPK activator, stimulates the phosphorylation of aquaporin 2 and urea transporter A1 in inner medullary collecting ducts. *Am J Physiol Renal Physiol*. 2016;310:F1008-F1012.
42. Al-Bataineh MM, Li H, Ohmi K, et al. Activation of the metabolic sensor AMP-activated protein kinase inhibits aquaporin-2 function in kidney principal cells. *Am J Physiol Renal Physiol*. 2016;311:F890-F900.
43. Liwang JK, Ruiz JA, LaRocque LM, Rianto F, Ma F, Wang Y. Role of PKC and AMPK in hypertonicity-stimulated water reabsorption in rat inner medullary collecting ducts. *Am J Physiol Renal Physiol*. 2019;316:F253-f262.
44. Cohen D, Musch A. Apical surface formation in MDCK cells: regulation by the serine/threonine kinase EMK1. *Methods*. 2003;30:269-276.
45. Cohen D, Brennwald PJ, Rodriguez-Boulan E, Musch A. Mammalian PAR-1 determines epithelial lumen polarity by organizing the microtubule cytoskeleton. *J Cell Biol*. 2004;164:717-727.
46. Suzuki A, Hirata M, Kamimura K, et al. aPKC acts upstream of PAR-1b in both the establishment and maintenance of mammalian epithelial polarity. *Curr Biol*. 2004;14:1425-1435.
47. Elbert M, Cohen D, Musch A. PAR1b promotes cell-cell adhesion and inhibits dishevelled-mediated transformation of Madin-Darby canine kidney cells. *Mol Boil Cell*. 2006;17:3345-3355.
48. Ducharme NA, Hales CM, Lapierre LA, et al. MARK2/EMK1/Par-1Balpha phosphorylation of Rab11-family interacting protein 2 is necessary for the timely establishment of polarity in Madin-Darby canine kidney cells. *Mol Boil Cell*. 2006;17:3625-3637.
49. Cohen D, Tian Y, Musch A. Par1b promotes hepatic-type lumen polarity in Madin Darby canine kidney cells via myosin II- and E-cadherin-dependent signaling. *Mol Boil Cell*. 2007;18:2203-2215.
50. Zeaiter Z, Cohen D, Musch A, Bagnoli F, Covacci A, Stein M. Analysis of detergent-resistant membranes of Helicobacter pylori infected gastric adenocarcinoma cells reveals a role for MARK2/Par1b in CagA-mediated disruption of cellular polarity. *Cell Microbiol*. 2008;10:781-794.
51. Lapierre LA, Avant KM, Caldwell CM, et al. Phosphorylation of Rab11-FIP2 regulates polarity in MDCK cells. *Mol Boil Cell*. 2012;23:2302-2318.
52. Lazaro-Dieguez F, Cohen D, Fernandez D, Hodgson L, van Ijzendoorn SC, Musch A. Par1b links lumen polarity with LGN-NuMA positioning for distinct epithelial cell division phenotypes. *J Cell Biol*. 2013;203:251-264.
53. Lapierre LA, Manning EH, Mitchell KM, Caldwell CM, Goldenring JR. Interaction of phosphorylated Rab11-FIP2 with

Eps15 regulates apical junction composition. *Mol Boil Cell*. 2017;28:1088-1100.
54. McRae R, Lapierre LA, Manning EH, Goldenring JR. Rab11-FIP1 phosphorylation by MARK2 regulates polarity in MDCK cells. *Cell Logist*. 2017;7:e1271498.
55. Ohno S. Intercellular junctions and cellular polarity: the PAR-aPKC complex, a conserved core cassette playing fundamental roles in cell polarity. *Curr Opin Cell Biol*. 2001;13:641-648.
56. Katsura T, Gustafson CE, Ausiello DA, Brown D. Protein kinase A phosphorylation is involved in regulated exocytosis of aquaporin-2 in transfected LLC-PK1 cells. *Am J Physiol Renal Physiol*. 1997;272:F817-F822.
57. Bradford D, Raghuram V, Wilson JL, et al. Use of LC-MS/MS and Bayes' theorem to identify protein kinases that phosphorylate aquaporin-2 at Ser256. *Am J Physiol Cell Physiol*. 2014;307:C123-139.
58. Bouley R, Breton S, Sun T, et al. Nitric oxide and atrial natriuretic factor stimulate cGMP-dependent membrane insertion of aquaporin 2 in renal epithelial cells. *J Clin Invest*. 2000;106:1115-1126.
59. Douglass J, Gunaratne R, Bradford D, et al. Identifying protein kinase target preferences using mass spectrometry. *Am J Physiol Cell Physiol*. 2012;303:C715-727.
60. Procino G, Carmosino M, Marin O, et al. Ser-256 phosphorylation dynamics of Aquaporin 2 during maturation from the ER to the vesicular compartment in renal cells. *FASEB J*. 2003;17:1886-1888.
61. Prats C, Helge JW, Nordby P, et al. Dual regulation of muscle glycogen synthase during exercise by activation and compartmentalization. *J Biol Chem*. 2009;284:15692-15700.
62. Mohammadi A, Perry RJ, Storey MK, Cook HW, Byers DM, Ridgway ND. Golgi localization and phosphorylation of oxysterol binding protein in Niemann-Pick C and U18666A-treated cells. *J Lipid Res*. 2001;42:1062-1071.

SUPPORTING INFORMATION

Additional supporting information may be found online in the Supporting Information section.

How to cite this article: Datta A, Yang C-R, Limbutara K, et al. PKA-independent vasopressin signaling in renal collecting duct. *The FASEB Journal*. 2020;00:1–18. https://doi.org/10.1096/fj.201902982R